



HAL
open science

Tomographic method for evaluation of apparent activation energy of steady-state creep

Federico Sket, Kristof Dzieciol, Augusta Isaac, Andras Borbely, Ar Pyzalla

► To cite this version:

Federico Sket, Kristof Dzieciol, Augusta Isaac, Andras Borbely, Ar Pyzalla. Tomographic method for evaluation of apparent activation energy of steady-state creep. *Materials Science and Engineering: A*, 2010, 527 (7-8), pp.2112-2120. 10.1016/j.msea.2009.11.058 . hal-00855062

HAL Id: hal-00855062

<https://hal.science/hal-00855062>

Submitted on 17 Aug 2022

HAL is a multi-disciplinary open access archive for the deposit and dissemination of scientific research documents, whether they are published or not. The documents may come from teaching and research institutions in France or abroad, or from public or private research centers.

L'archive ouverte pluridisciplinaire **HAL**, est destinée au dépôt et à la diffusion de documents scientifiques de niveau recherche, publiés ou non, émanant des établissements d'enseignement et de recherche français ou étrangers, des laboratoires publics ou privés.



Distributed under a Creative Commons Attribution - NonCommercial 4.0 International License

Tomographic method for evaluation of apparent activation energy of steady-state creep

F. Sket^{b,*}, K. Dzieciol^a, A. Isaac^b, A. Borbély^a, A.R. Pyzalla^b

^a Max-Planck-Institut für Eisenforschung GmbH, Max-Planck-Strasse 1, 40237 Düsseldorf, Germany

^b Helmholtz Centre Berlin for Materials and Energy GmbH, Glienicker Strasse 100, 14109 Berlin, Germany

A new method for the evaluation of the apparent activation energy of steady-state creep in metals is pre-sented. It is based on in situ monitoring by microtomography the geometry of a specimen subjected to uniaxial load and inhomogeneous temperature distribution. It is shown that microtomography acting as a three dimensional extensometer enables the evaluation of local strain-rates of small material volumes and is an adequate tool for characterization of inhomogeneously deforming specimens. Activation ener-gies obtained with the new method for stainless steel agree within an error of 5% with values obtained according to the classical procedure.

1. Introduction

Creep deformation of metals at temperatures higher than about 1/3rd of the melting temperature T_m is governed by several thermally activated processes enhancing dislocation motion and recovery, diffusion of vacancies as well as dynamic recrystallization [1]. These mechanisms influence mainly stage II of creep, where specimens under constant stress deform usually at nearly constant strain-rate. The relationship between this steady-state strain-rate and stress in pure metals and Class M alloys is often described by a power-law function [1,2]:

$$\dot{\epsilon}_{ss} = C \cdot \left(\frac{\sigma}{G(T)} \right)^n \cdot \exp \left(- \frac{Q_a}{R \cdot T} \right). \quad (1)$$

The pre-exponential factor C comprises structure-dependent parameters and is usually considered constant [3]. $\sigma/G(T)$ is the shear modulus normalized stress (some authors are using the Young's modulus $E(T)$), n is the stress exponent, R is the gas constant and Q_a is the apparent activation energy of steady-state creep. The key parameters of this phenomenological description are n and Q_a , which once evaluated give good hints about the main creep mechanism. It is the aim of the present work to present a new evaluation method of Q_a based on in situ microtomography. Before present-

ing the new method, however, the usual evaluation procedures are recalled.

Based on Eq. (1) the apparent activation energy for creep is defined as follows:

$$Q_a = -R \cdot \left[\frac{\partial(\ln \dot{\epsilon})}{\partial(1/T)} \right]_{\sigma/G, s}, \quad (2)$$

where σ/G and "s" indicate that the data should represent constant normalized stress and constant structure conditions. In practice several creep tests at constant normalized-stress and different temperatures are performed and Q_a is obtained from the slope of the line fitting the steady-state creep-rates vs. the inverse of temperature ($1/T$). Nix et al. [4] have compiled the activation energies of creep for a large class of materials and compared them with the corresponding activation energies of lattice self-diffusion, Q_{sd} . They have shown that the two quantities are essentially equal, which supports the idea that the mechanism of five-power-law creep (with stress exponent $n \approx 5$) is strongly related to diffusion of vacancies. Sherby et al. [5], using the same classical method, have obtained the activation energy of pure aluminum over a large range of temperatures, from about $0.3 T_m$ to $0.9 T_m$. Their results confirm that above $0.6 T_m$, Q_a is comparable to that of lattice self-diffusion, but below $0.6 T_m$ is smaller than Q_{sd} . Luthy et al. [6] obtained similar results for aluminum from torsion creep tests over a range of temperatures from about $0.29 T_m$ to $0.93 T_m$.

The definition of activation energy (Eq. (2)) indicates that only tests performed at constant normalized stress, $\sigma/G(T)$ and

* Corresponding author. Tel.: +49 211 6792 164; fax: +49 211 6792 390.
E-mail address: f.skett@mpie.de (F. Sket).

characterized by identical structures can be used for evaluation. This requirement seems to be partly satisfied already by tests performed at constant $\sigma/G(T)$, when the average subgrain size and average distance between free dislocations were found to obey a power-law relationship with $\sigma/G(T)$ [7]. Subgrain misorientations, however, are not constant and slightly evolve with strain [8]. Importance of subgrain boundaries can be related to their role played in the recovery of free dislocations, which controls the creep rate [9]. This indicates that samples at different temperatures and strains have slightly different structures and suggests that an evaluation method based on one single specimen is more adequate [10–12]. Since temperature appears in the exponent of Eq. (1) a small temperature change can have a large effect on the strain-rate. Therefore applying a small temperature jump $\Delta T = T_2 - T_1$ will considerably change the creep rate from $\dot{\epsilon}_1$ to $\dot{\epsilon}_2$. If the structure does not change much for the ΔT jump the creep rates and temperatures can be related as [10–12]:

$$R \cdot \ln \left(\frac{\dot{\epsilon}_1}{\dot{\epsilon}_2} \right) = Q_a \cdot \left(\frac{1}{T_2} - \frac{1}{T_1} \right). \quad (3)$$

The procedure can be repeated several times for different temperature jumps and the activation energy can be obtained from the slope of the line fitted to the logarithm of strain-rate ratios as a function of the difference of the inverse temperatures (Eq. (3)). Activation energies evaluated according to this method for Al, Cu and Ni were published by Refs. [13,14]. The values for Al above $0.6 T_m$ are by about 7% higher than those obtained by the classical method [5,6].

Based on the concept that the effective stress (σ^*) acting on a moving dislocation is the difference between the applied stress σ and the internal stress σ_i created by neighboring dislocations and other obstacles, Ahlquist et al. [15] have proposed two other definitions of the activation energy Q^* and Q_i (with equations similar to Eq. (2)) at constant effective stress and internal stress, respectively. The former energy characterizes dislocation glide, while the latter the recovery process [15]. Dobeš and Milička [16] have suggested the determination of the activation energy at the same structural state, i.e. at an identical level of the internal stress, and at the same applied stress:

$$Q_i^* = -R \left[\frac{\partial \ln \dot{\epsilon}_s}{\partial (1/T)} \right]_{\sigma_i, \sigma}. \quad (4)$$

They have argued (using experimental data for the aluminum alloy Al–13.7 wt.% Zn) that the extrapolated value of Q_i^* to zero applied stress becomes identical to the apparent activation energy of creep obtained from classical tests. The constant structural stress state condition in this definition resembles the constant structure condition of Eq. (2).

More recently, Synchrotron X-ray Microtomography (SXR) has emerged as a powerful technique [17–24] that enables a three dimensional (3D) characterization of heterogeneous microstructures and specimen's shape. The non-destructive nature of this technique associated with an adequate time resolution provides new possibilities for in situ characterization of creep. The high resolution achievable with microtomography turns this technique into an excellent tool for the evaluation of local deformations at the micrometer scale especially for inhomogeneous conditions. It is the aim of the present investigation to demonstrate the adequacy of in situ tomography for the evaluation of activation energy of creep. The method is exemplified on stainless steel specimens deformed under two different conditions and the tomographic outcome is compared with results of the traditional method.

2. Experimental details

2.1. Specimen geometry adapted to tomographic measurement conditions

Test specimens were specially developed to meet the requirements of the tomographic set-up at ID15A of the European Synchrotron Radiation Facility (ESRF), which was equipped with a CCD camera having a restricted field of view of about $1.2 \text{ mm} \times 1.1 \text{ mm}$. The effective pixel size of the detector was $1.6 \mu\text{m}$ and had a resolution of about $2 \mu\text{m}$ (the full width at half maximum of the point spread function). The tomograms were recorded using a high-energy beam ($\sim 80 \text{ keV}$) with a large bandwidth ($\sim 50\%$). The geometry of the investigated specimens is shown in Fig. 1 and has the diameter and the gauge length (L) of about 1 mm. Fig. 1 also shows the position of the illuminated volume in the sample and its reconstruction by tomography. The reconstructed volume is constituted of voxels, each voxel representing a volume of $1.6^3 \mu\text{m}^3$. The specimens are designed with threads at both ends which are screwed in at one end into the load cell and at the other end into the reaction yoke of the creep machine. The specimens have two small holes placed 4 mm apart from the center of the sample where thermocouples for temperature measurement are placed (T1 and T2). The elongation of the sample is measured with an inductive displacement transducer (Fig. 2) attached with the head of the load cell. Recording of data as well as the control of the machine are made through computer.

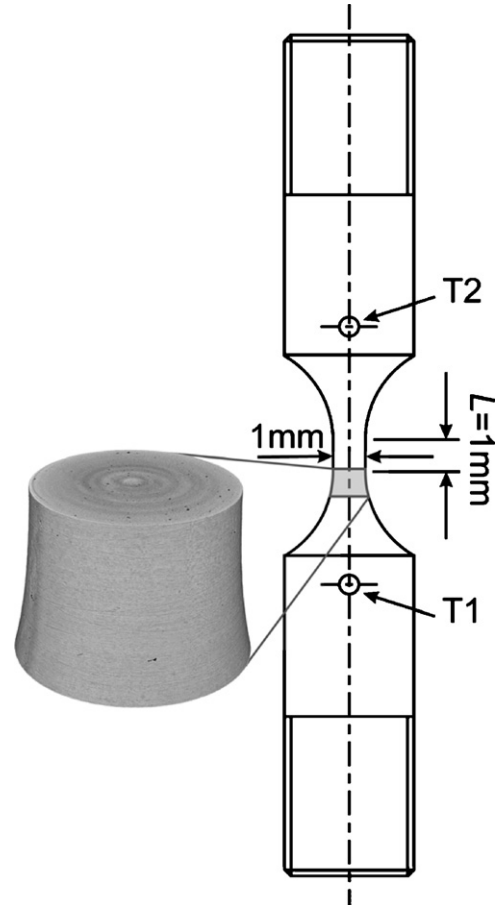


Fig. 1. Schematic drawing of the specimen used for in situ investigations, illuminated volume in the sample and its reconstruction by tomography.

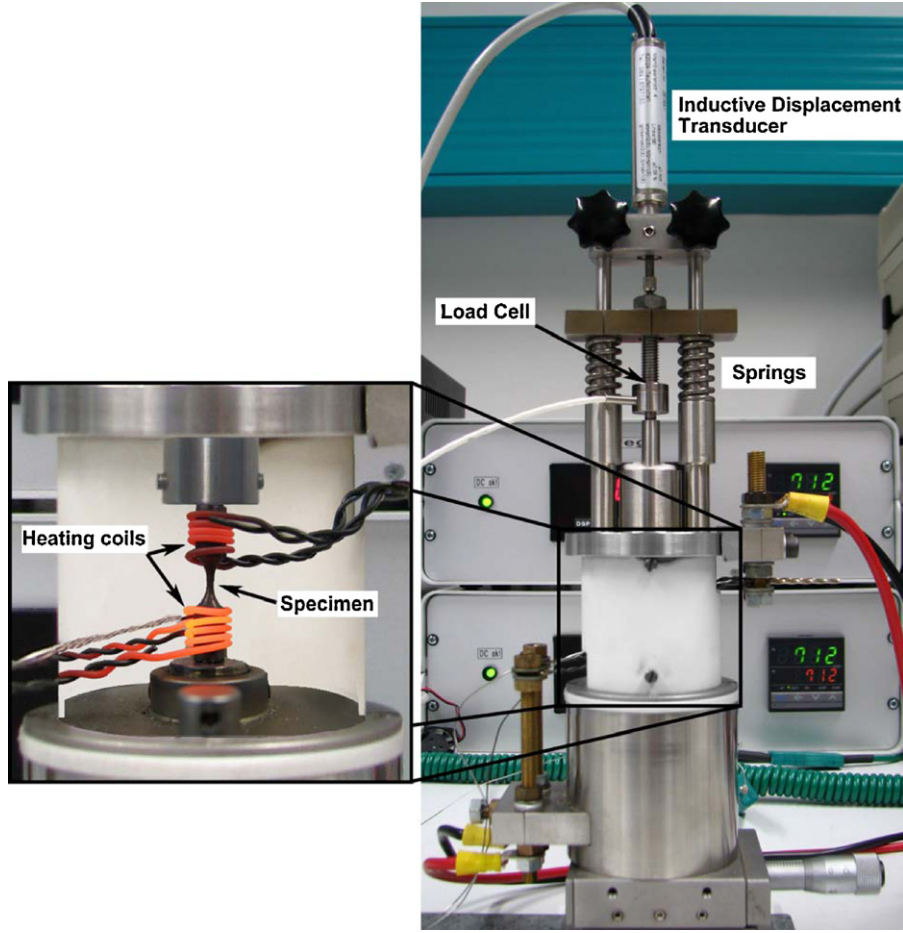


Fig. 2. Creep machine for in situ measurements.

2.2. Creep tests under nearly constant load or stress

The load is applied to the specimen via two springs (material spring steel 1.1200 Class C) with proper constant to achieve the required stress value. When the springs are compressed the load is transferred to the sample through the load cell, which measures the actual load applied to the specimen. The whole loading system is mounted on a ceramic tube with good creep resistance at high temperatures and transparent to high-energy beams. By a proper selection of the spring constant nearly constant load or constant stress conditions can be applied. Evidently the elongation of the sample produces a load change by the expansion of the springs, however, this change can be kept below a certain tolerance by selecting a proper spring constant. The admissible relative load change or *tolerance* is defined as follows:

$$\Delta F = \frac{F_0 - F_r}{F_0} = \frac{x_0 - x_r}{x_0} \leq \text{tolerance}, \quad (5)$$

where F_0 and F_r are the loads at the beginning and at the end of the creep test and x_0 and x_r the corresponding compression lengths of the springs. The maximum spring constant fulfilling this criterion is obtained as:

$$k_{\max} = \frac{\sigma_0 \cdot A_0 \cdot \text{tolerance}}{N_s \cdot l_0 \cdot (e^{\varepsilon_r} - 1)}, \quad (6)$$

where l_0 is the initial length of the sample, A_0 the initial cross-section, σ_0 the initial stress, N_s the number of springs and ε_r the strain to rupture. In our experiments usually a tolerance of 5% was selected.

A test at nearly constant stress becomes also possible if the relaxation of the load due to the elongation of the springs equals the decrease in load due to the decrease of cross-sectional area (assuming the stress constant) of the specimen. The equal stress condition will be valid at two strains, which can be adequately selected for example at the beginning and at the end of secondary creep regime. The following general condition can be written:

$$\sigma(\varepsilon_1) = \sigma(\varepsilon_2), \quad (7)$$

where ε_1 and ε_2 are the selected strains. Assuming that the volume of the sample remains constant during deformation, the initial compression x_0 of the spring can be worked out:

$$x_0 = l_0 \frac{(e^{\varepsilon_2} - 1) \cdot e^{\varepsilon_2} - (e^{\varepsilon_1} - 1) \cdot e^{\varepsilon_1}}{e^{\varepsilon_2} - e^{\varepsilon_1}}, \quad (8)$$

with l_0 being the initial gauge length.

The spring constant is determined by the selected stress σ_0 and is given by:

$$k = \frac{\sigma_0 \cdot A_0}{N_s \cdot e^{\varepsilon_i} \cdot (x_0 - l_0 \cdot (e^{\varepsilon_i} - 1))}, \quad (9)$$

where ε_i denotes either ε_1 or ε_2 . Selecting for example the strains $\varepsilon_1 = 0.08$ and $\varepsilon_2 = 0.3$ where the equal stress condition is imposed it can be shown that the relative stress variation in the $[0, 0.35]$ strain interval is less than 2%.

2.3. Testing conditions

The high temperature necessary for creep was imposed by two resistive heating coils placed around the ends of the sam-

Table 1

Chemical composition (wt.%) of the investigated stainless steel AISI 440B.

C	Si	Mn	P	S	Cr	Mo	V
0.85–0.95	≤1.00	≤1.00	≤0.04	≤0.015	17.0–19.0	0.90–1.30	0.07–0.12

Table 2Measurement conditions of in situ experiments. Applied stress σ , temperature at the bottom of the sample T_b , measured temperature difference between calibration points ΔT , temperature gradient in region with constant cross-section ∇T , minimum strain-rate $\dot{\epsilon}_{ss}$ and rupture time t_r .

Sample	σ [MPa]	T_b [K]	ΔT [K]	∇T [K/mm]	$\dot{\epsilon}_{ss}$ [1/s]	t_r [h]
A	180	985 ± 1	624 ± 2	99	3.1 × 10 ⁻⁶	24.7
B	210	1013 ± 1	645 ± 2	105	1.2 × 10 ⁻⁵	7.9

ple (Fig. 2). At the position of each heating coil thermocouples measure the temperature and a proportional-integral-derivative (PID) controller is used to keep the imposed temperature within ±1 K. Asymmetric heating becomes possible by setting different temperatures for the two coils, making possible tests with a temperature distribution (sample regions with constant cross-sectional area experiencing a constant gradient in this case). The tomographic investigations were performed on a commercial stainless steel AISI 440B with chemical composition given in Table 1. Two experiments with asymmetric heating (with upper coil switched off) were performed at stress values of 180 MPa and at 210 MPa, which correspond to the minimum creep rate of the samples A and B, respectively. The detailed conditions of the experiments are given in Table 2.

2.4. Image correlation for evaluation of tomographic data

The tomographic reconstructions as well as their processing were done with in-house software written in Interactive Data Language (IDL) and Matlab. To monitor changes in the sample's shape, material slices (height of 1 voxel) lying perpendicular to the stress axis were chosen, which due to the axial symmetry of the experiment will move during creep along this axis. Slice displacement was evaluated by cross correlating a selected slice from the initial volume with slices from consecutive reconstructions. The most sensitive correlation indicator was found to be the product between the amplitude of the inverse cross-power spectrum of the correlated images and the classical cross-correlation coefficient [25]. Once the displacement of a slice was found, the corresponding local true strain could be calculated as the logarithm of the ratio between slice area in the reference and actual configurations. For higher accuracy an average strain over 10 slices making up a slab was calculated. Selecting a slab as structural unit for evaluations was imposed also by the nearly constant temperature condition required in the slab in the time interval selected for evaluation. Usually the difference in temperature between the lower and upper slice of the slab is larger than the average temperature change of the slab over the selected time interval.

3. Method for Q_a evaluation exemplified on experimental data

3.1. In situ creep curves

The overall creep curves for samples A and B are plotted in Fig. 3a and b, respectively, together with the local creep curves of the material slabs. The thick solid lines are the curves calculated from the total displacement of the samples (during the in situ measurement) considering an effective length of 1.8 mm as defined in Section 4.2. The local curves (gray lines with symbols) were obtained from tomographic evaluations by averaging the local strain over the slices making up the slab. The reference state for cal-

ulation of the local creep curves was considered at time 852 min and 156 min for sample A and B, respectively. For easier comparison the local creep curves were shifted vertically to bring them together with the overall curves. The insert in Fig. 3a serves this purpose, too. The different creep behavior of the slabs is primarily due to the temperature gradient leading to inhomogeneous strain distribution in the sample, i.e. the creep behavior of local material slabs will differ from the overall behavior of the sample. Fig. 3c and d shows the global strain-rates as a function of time for samples A and B, respectively. Sample A experiences a long primary creep regime in which the strain-rate decreases continuously reaching a steady-state after about 15 h. For sample B, deformed at higher stress and higher temperatures, a short transient regime with increasing and decreasing strain-rate is observed between 60 and 120 min of the creep test. Such transient was also observed during creep of a small brass sample [26]. All tomographic evaluations as well as the evaluation of the activation energy of creep are focused on the secondary regime, when a nearly steady-state in the whole sample and in local material slabs was reached.

3.2. Temperature distribution calibration

The temperature distribution in the specimen was calibrated through finite element (FE) calculations taking into account the accurate shape of the sample and the temperatures measured by the thermocouples. The calculations were performed for thermal steady-state using the following material constants: heat conductivity $\lambda = 24.2 \text{ W/m K}$, specific heat $c = 460 \text{ J/kg K}$ and mass density $\rho = 7650 \text{ kg/m}^3$. Fig. 4 shows the temperature distribution in samples A and B as a function of the distance from the center of the specimens. There is a non-linear temperature variation in regions with varying cross-section, while in the middle of the samples, where the cross-section is practically constant the temperature changes linearly with distance. Based on temperature profiles obtained from FE simulations a certain average temperature and a corresponding tolerance can be now ascribed to each slab. It will be shown later that the temperature change of one slab during the short strain interval considered for the evaluation of Q_a is small and the error in temperature is mainly determined by its variation over the slab's height.

3.3. Evaluation of the apparent activation energy Q_a

Applying Eq. (1) to two slabs one located at a reference temperature T_0 (usually the smallest temperature in the analyzed region) and the second at temperature T , the ratio of the corresponding strain-rates can be written as follows:

$$\ln \left[\frac{\dot{\epsilon}(T, t)}{\dot{\epsilon}(T_0, t)} \cdot \left(\frac{\sigma(T_0, t)}{\sigma(T, t)} \right)^n \cdot \left(\frac{G(T)}{G(T_0)} \right)^n \right] = Q_a \cdot \left(\frac{\Delta T}{R \cdot T_0 \cdot T} \right), \quad (10)$$

where $\Delta T = T - T_0$. The local strains (and strain-rates) are obtained from tomographic reconstructions performed at the reference time

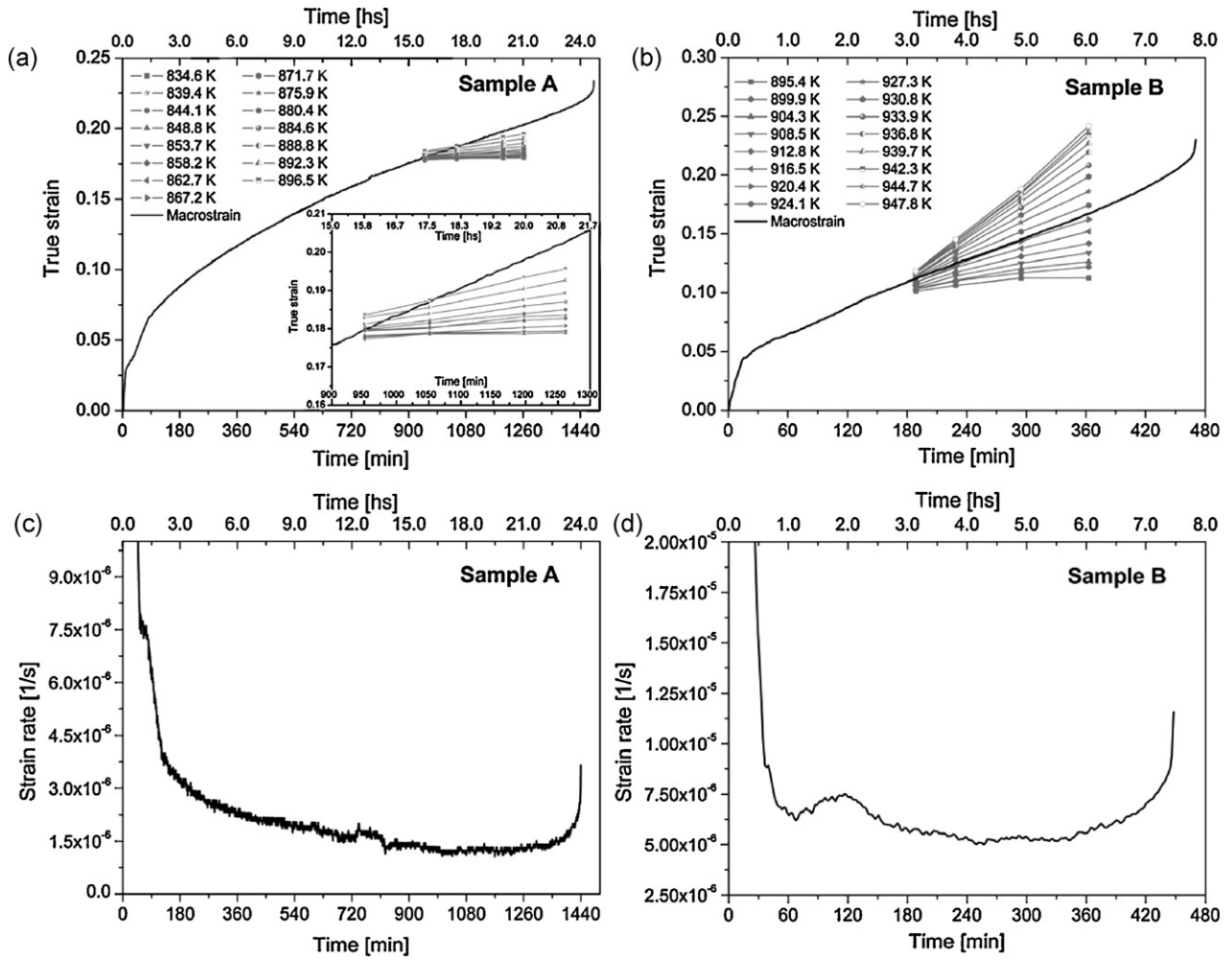


Fig. 3. Overall creep curves for samples A and B (thick solid lines) together with creep curves of local material slabs (gray lines with symbols) obtained from tomographic evaluations (a) and (b). Overall creep rate vs. time for sample A (c) and B (d).

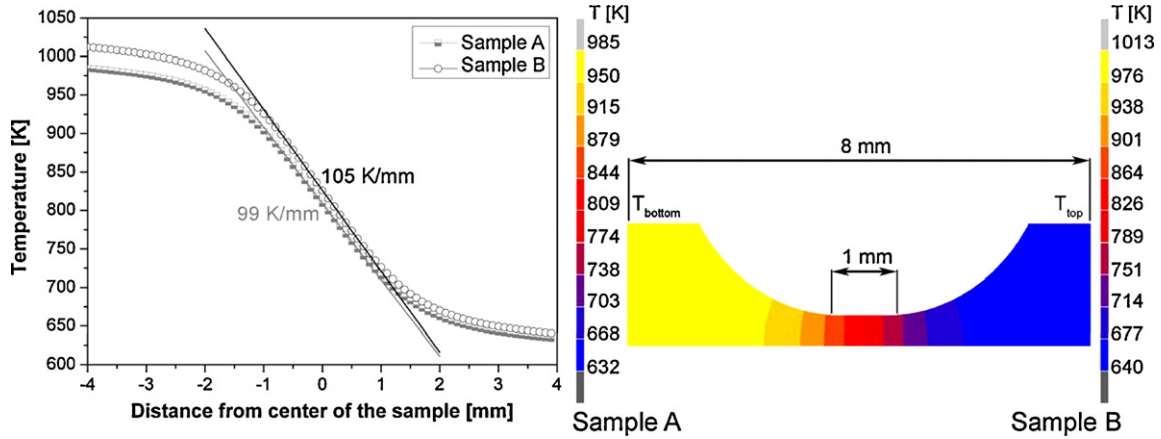


Fig. 4. Temperature profiles along the stress axis as obtained from FE simulations for samples A and B.

t_0 and current time t . Assuming that the volume of the creeping material is constant the local strain in the slab can be related to the local change in sample's cross-section as:

$$\varepsilon(T, t) = \ln \left(\frac{A(T, t_0)}{A(T, t)} \right), \quad (11)$$

while the local strain-rate in the time interval $\Delta t = t_2 - t_1$ (and associated to time t_2) is given by:

$$\begin{aligned} \dot{\varepsilon}(T, t_2) &= \frac{\varepsilon(T, t_2) - \varepsilon(T, t_1)}{\Delta t} = \frac{1}{\Delta t} \left[\ln \left(\frac{A(T, t_0)}{A(T, t_2)} \right) - \ln \left(\frac{A(T, t_0)}{A(T, t_1)} \right) \right] \\ &= \frac{1}{\Delta t} \ln \left(\frac{A(T, t_1)}{A(T, t_2)} \right), \end{aligned} \quad (12)$$

where $A(T, t)$ is the average area of the slab at temperature T and time t . It is important to note that evaluation of the strain-rate at time t_2 does not require the measurement of the initial state (at

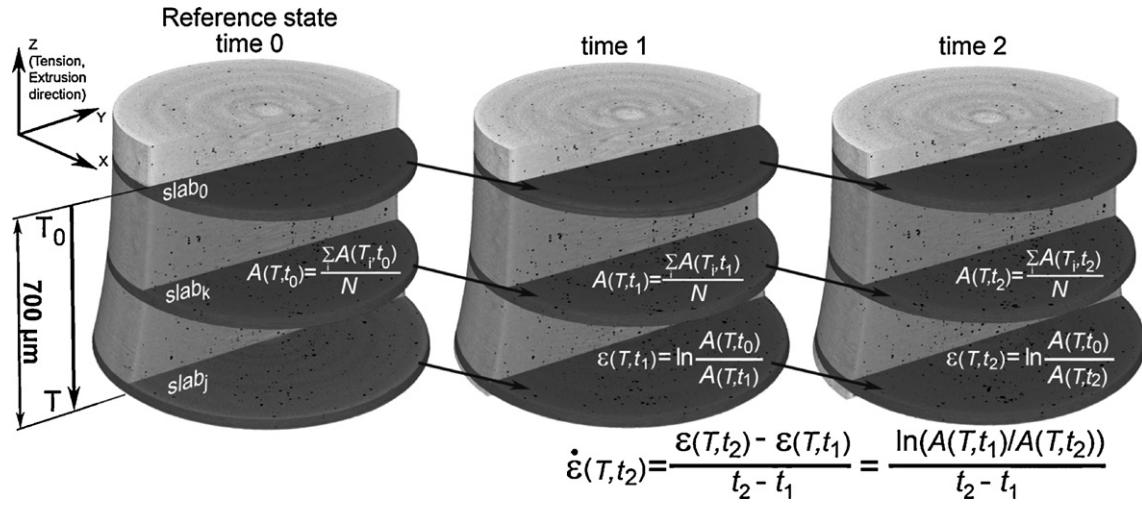


Fig. 5. Examples of slab displacement along the tensile axis and the methodology of strain and strain-rate calculation for the slab. N represents the number of slices in the slab.

time t_0) but only the state at time t_1 . However, if the local creep curves are of interest then the reference state is also required. Fig. 5 exemplifies the position change of three slabs during creep and the methodology used for strain evaluation.

Considering a sample with constant cross-section in the reference state it becomes possible within certain conditions to evaluate Q_a without knowing the stress exponent n . The method was already applied to evaluation of Q_a in brass (with $n=3.4$) and good agreement with literature data was obtained [27]. Usually in practice not only volumes with constant cross-section are reconstructed, but also regions with varying section (see Fig. 5) where the stress is slightly changing. The stress ratio in Eq. (10) can be expanded in a series of the strain difference between slabs at temperatures T and T_0 from which keeping only the first terms we get:

$$\left[\frac{\sigma(T_0, t)}{\sigma(T, t)} \right]^n = \left[\frac{A(T, t)}{A(T_0, t)} \right]^n \cong 1 - n(\varepsilon(T, t) - \varepsilon(T_0, t)), \quad (13)$$

This equation suggests that the stress ratio approaches 1 if the strain difference between slabs is small. This condition is usually fulfilled in case of small temperature gradients, when the ratio of the shear moduli approaches unity, too. Considering the stress exponent n to be known, Eq. (10) suggests that Q_a can be determined even in such cases, however, only with the restriction that the cross-sectional area of the slices does not vary fast and the assumption of a uniaxial stress state is approximately fulfilled. In case of present

experiments the stress triaxiality in the investigated region with varying cross-section was below 0.38.

4. Results and discussion

4.1. Q_a values according to classical and tomographic methods

The creep behavior of the AISI 440B steel was first investigated by the conventional method on large specimens. The stress exponent n was evaluated from the slope of $\ln(\dot{\varepsilon}_{\min})$ vs. $\ln(\sigma)$ obtained from tests at constant temperature 873 K (see Fig. 6a). Additionally, the activation energy corresponding to the minimum creep-rate was obtained from tests performed at different temperatures for two different normalized stress values of 1.4×10^{-3} and 3.1×10^{-3} (σ of about 77 MPa and 180 MPa, respectively). The corresponding linear fits performed on the plot of $-R \cdot \ln(\dot{\varepsilon}_{\min})$ as function of $1/T$ yielded the values of $Q_a = 388 \pm 15$ kJ/mol and 389 ± 17 kJ/mol for the small and large normalized stress, respectively. This means that Q_a does not depend on stress in the studied interval, which is in good agreement with literature data for stainless steel [28].

For the analysis of tomographic data it is preferred to plot the left hand side of Eq. (10) against $\Delta T/(R \cdot T_0 \cdot T)$. When $\Delta T \ll T_0 \cong T$ then the left hand side of Eq. (10) becomes a linear function of ΔT and the fitted line should intersect the origin, too. Fig. 7a and b shows

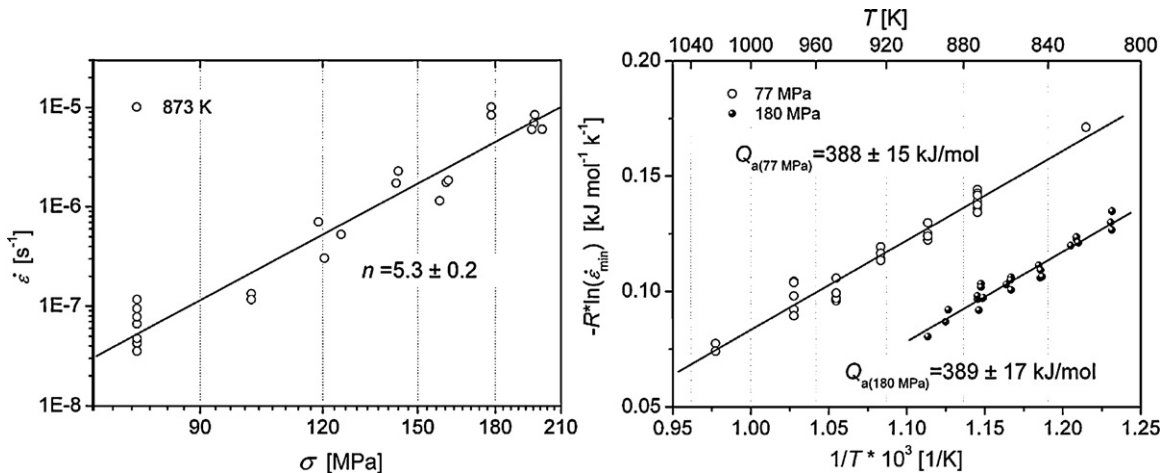


Fig. 6. Evaluation of the stress exponent n (a) and activation energy of steady-state creep (b) from laboratory tests according to the conventional method.

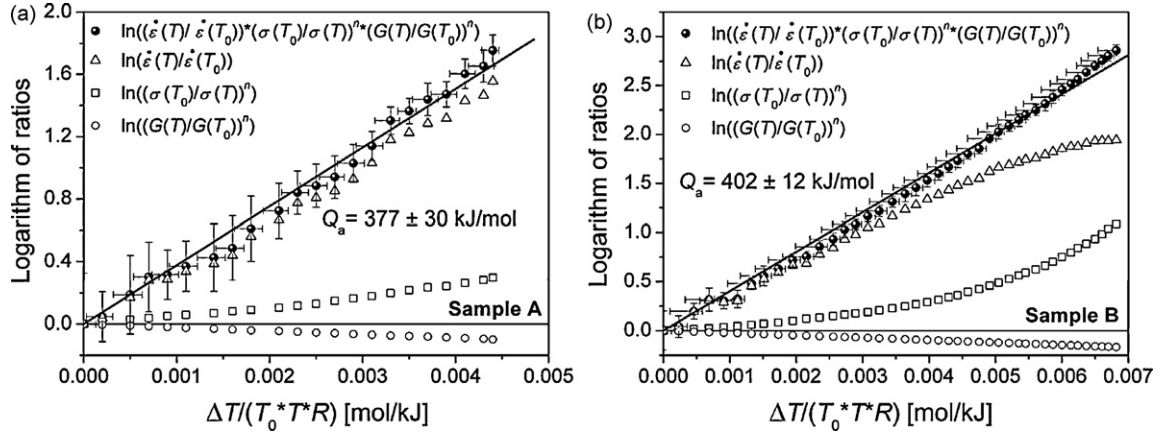


Fig. 7. Linear regressions performed on tomographic data to obtain Q_a ; (a) sample A and (b) sample B. The diagrams also show the contributions of different ratios entering Eq. (10). The sum of the three functions gives the left hand side of Eq. (10).

the variation with temperature of the parameter-ratios entering Eq. (10) namely, that of the strain-rates, stresses and shear moduli. It is evident that the main contribution comes from the ratio of the strain-rates and the other two should be considered as correction factors with decreasing importance. Neglecting for example the shear modulus correction, has an effect of less than 5% on Q_a . The slopes of the fitted lines (Fig. 7a and b) give activation energies equal to 377 ± 30 kJ/mol and 402 ± 12 kJ/mol for samples A and B, respectively. These values are equal within experimental error with each other and with the result obtained according to the conventional method. We note that the error of Q_a can be further reduced by increasing the resolution of the tomographic reconstruction. For high-energy beams, however, detectors with better efficiency are needed to pass the actual resolution of about $2 \mu\text{m}$.

4.2. Comparison of strain distribution in the real sample and FE models

The overall strain is a macroscopic quantity characteristic for the whole sample. Due to the restricted field of view of the CCD camera, tomography gives information only from a portion of the gauge length and the average “tomographic” strain might not coincide with the strain calculated from the measured displacement of the sample’s top (Fig. 3a and b). In order to check if the local strain distribution delivered by tomography matches the strain distribution in homogeneous material FE simulations have been performed. The comparison is shown in Fig. 8a and b for the two samples A and B, respectively. The contour plots and the above located diagrams clearly show that the maximum strain regions are shifted towards higher temperatures (negative position values in Fig. 8a and b) which, however, were not captured by tomography. The regions evaluated are indicated by vertical lines and are confined to the interval $[-0.67, -0.05]$ mm for sample A and $[-0.90, -0.41]$ mm for sample B. The inserts in the upper right corner of the figures show the strain distribution obtained from tomography at different creep times. The continuous black line with full squares depicts the distribution at the end of steady-state. In FE simulations a Norton law describing steady-state creep with appropriate constants for the investigated steel was used and deformation was simulated until the elongation of the sample reached the value describing the end of secondary stage. The strain distribution obtained from FE simulations facilitates a better understanding and design of the in situ experiment. It becomes evident that the field of view of the CCD should be positioned in the sample region with the highest strain gradient, when the ratio of strain-rates $(\dot{\epsilon}(T, t)/\dot{\epsilon}(T_0, t))$ becomes the largest and less affected by experimental errors.

The strain distribution obtained from FE calculations allows introducing an “effective length”, a quantity that facilitates the calculation of the average strain and the overall creep curve. In case of tests performed at constant temperature the strain distribution along the sample axis can be well described by a Gaussian function. For asymmetric heating the distribution becomes asymmetric, which suggests selecting a criterion based on the relative amount of strain present in a given volume around the center of the strain profile. The average strain in the sample of length L is obtained as follows:

$$\bar{\epsilon} = \frac{1}{L} \int \epsilon(z) dz = \frac{U_{\text{exp}}}{L}, \quad (14)$$

where the integration is performed over L and U_{exp} is the measured displacement. Since the strain is localized in a small region, using L as the effective length is not adequate. Therefore we define an effective length L_{eff} equal with the interval around the center of the strain profile, which contributes by 95% to the total elongation of the sample. The L_{eff} was evaluated from strain profiles obtained from FE simulations and its value is about 1.8 mm, almost twice the gauge length of the sample with constant cross-section. The average strain (and strain-rate) shown in Fig. 3 were calculated according to Eq. (14) considering $L = 1.8$ mm. We note, however, that the value of Q_a is not affected by the selected L_{eff} , which affects only the overall curves.

4.3. Error estimation

For every new evaluation method it is important to characterize the sources of error influencing the final results. The resolution of the tomographic reconstruction is of about $2 \mu\text{m}$, which in case of a sample with diameter equal to 1 mm, gives a relative error of the local strain and strain-rate below 1% (the uncertainty in determining the diameter is considered equal with the tomographic resolution). This is much smaller than the standard deviation of the average strain (and strain-rate) of one slab, of about 12%, determined by the different creep behavior of the slices making up the slab. The stress ratio in Eq. (10) reduces also to the ratio of two areas and consequently it has the same relative error.

Another source of uncertainty is related to the local temperature calibration obtained from FE simulations. Selecting a slab (instead of a slice) as structural unit the error of the temperature associated to the slab depends on the location of the slab (through the local temperature gradient and local displacement) and the number of slices included. In case of samples A and B the slabs were considered to be made up of 10 slices, which gave maximum tem-

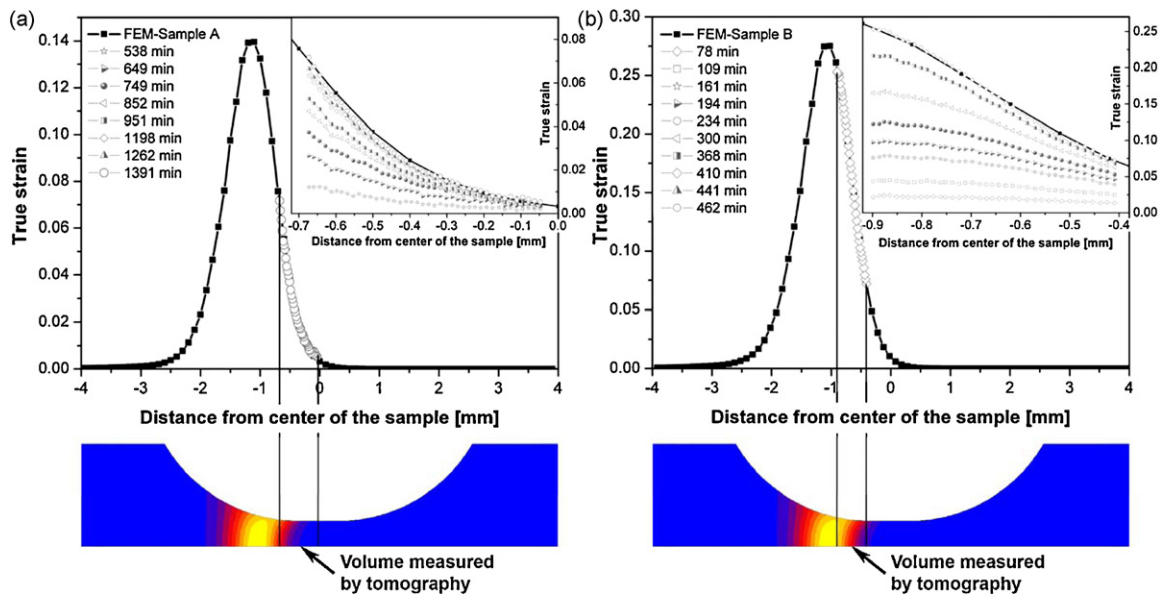


Fig. 8. Strain distribution (obtained from FE simulations) along the load axis of the specimens characterizing the end of steady-state (a) sample A and (b) sample B. The upper part in each figure shows the asymmetric strain distribution. The volume measured by tomography is marked by vertical lines. The inserts in the upper right corners show the strain distribution in the sample at stages where the tomographic reconstructions were performed.

perature errors of ± 0.8 K and ± 0.9 K, respectively. The temperature error due to sample elongation during steady-state creep was estimated based on the experimentally detected displacement for the uppermost slab in the reconstruction and the temperature gradient in the specimen at the beginning of steady-state. The total analyzed creep strain in sample A was 2.3% ($\Delta t = 310$ min) and 5.5% ($\Delta t = 174$ min) in sample B. These lead to a temperature change of the uppermost slab of about 0.3 K and 1.5 K for specimens A and B, respectively. Since the slabs are moving upwards the temperature error becomes asymmetric. The total temperature errors are equal to +0.8 K and -1.1 K for sample A and +0.9 K and -2.4 K for sample B. These errors correspond to the slab with the highest location and compared to the total temperature difference in the analyzed volume of about 50 K are small. The acceptable accuracy of the local temperature and strain-rate ratios, as well as the large number of slabs analyzed, makes possible an accurate evaluation of the activation energy. Both values of Q_a obtained from in situ tests as well as the values obtained from conventional laboratory tests are equal within an error of 5%.

5. Conclusions

It was shown that in situ microtomography is an excellent method for investigation of specimens undergoing inhomogeneous deformation allowing a good characterization of the kinematics of steady-state creep. The good accuracy of the method is related to the use of powerful image correlation algorithms, which applied to 3D tomographic images precisely capture changes in specimen's shape. The possibility to apply different loads on the sample like temperature, electric or magnetic fields, shows the flexibility of the experiment, which in present case was performed in a five dimensional parameter space (three spatial dimensions, the temporal dimension and a temperature gradient).

Activation energies of steady-state creep obtained with the new tomographic method on small samples are in good agreement with values from conventional methods on large specimens. The good agreement has two reasons: (i) the tomographic method uses the true values of strain-rate and stress and (ii) the slabs chosen as structural unit to characterize the inhomogeneous deforma-

tion still contain a large number of dislocations and fulfill the conditions necessary to treat them on the basis of continuum mechanics.

Acknowledgement

The authors are grateful to the staff of ID15A for the help during the experiments.

References

- [1] M.E. Kassner, M.T. Pérez-Prado, *Fundamentals of Creep and Alloys*, Elsevier, San Diego, 2004.
- [2] M.E. Kassner, M.T. Pérez-Prado, *Prog. Mater. Sci.* 45 (2000) 1–102.
- [3] V. Levitin, *High Temperature Strain in Metals and Alloys*, Wiley-VCH Verlag GmbH & Co. KGaA, Weinheim, 2006.
- [4] W.D. Nix, B. Ilshner, in: P. Haasen, V. Gerold, G. Kostorz (Eds.), *Strength of Metals and Alloys*, Pergamon Press, Oxford, 1980.
- [5] O.D. Sherby, R.J. Klundt, A.K. Miller, *Metall. Trans. A* 8 (1977) 843.
- [6] H. Luthy, A.K. Miller, O.D. Sherby, *Acta Metall.* 28 (1980) 169–178.
- [7] W. Blum, *Mater. Sci. Eng. A* 319–321 (2001) 8–15.
- [8] K.-G. Tak, U. Schulz, G. Eggeler, *Mater. Sci. Eng. A* 510–511 (2009) 121–129.
- [9] W. Blum, P. Eisenlohr, *Mater. Sci. Eng. A* 510–511 (2009) 7–13.
- [10] R.E. Reed-Hill, R. Abbaschian, *Physical Metallurgy*, third ed., PWS-Kent, Boston, 1992.
- [11] F. Garofalo, *Fundamentals of Creep and Creep-rupture in Metals*, Macmillan, New York, 1965.
- [12] O.D. Sherby, T.A. Trozera, J.E. Dorn, *Proc. Am. Soc. Test. Mater.* 56 (1956) 789.
- [13] O.D. Sherby, J.L. Lytton, J.E. Dorn, *Acta Metall.* 5 (1957) 219.
- [14] P.R. Landon, J.L. Lytton, L.A. Shepard, J.E. Dorn, *Trans. ASM* 51 (1959) 900.
- [15] C.N. Ahlquist, R. Gasca-Neri, W.D. Nix, *Acta Metall.* 18 (1970) 663–671.
- [16] F. Dobés, K. Milička, *Mater. Sci. Eng. A* 462 (2007) 380–383.
- [17] L. Babout, E. Maire, R. Fougères, *Acta Mater.* 52 (2004) 2475–2487.
- [18] C.F. Martin, C. Jossierond, L. Salvo, J.J. Blandin, P. Cloetens, E. Boller, *Scripta Mater.* 42 (2000) 375–381.
- [19] A. Borbély, F.F. Csikor, S. Zabler, P. Cloetens, H. Biermann, *Mater. Sci. Eng. A* 367 (2004) 40–50.
- [20] G.C. Requena, P. Degischer, E.D. Marks, E. Boller, *Mater. Sci. Eng. A* 487 (2008) 99–107.
- [21] K.E. Thompson, C.S. Wilson, W. Zhang, *Powder Technol.* 163 (2006) 169–182.
- [22] T. Link, S. Zabler, A. Epishin, A. Haibel, M. Bansal, X. Thibault, *Mater. Sci. Eng. A* 425 (2006) 47–54.
- [23] A. Pyzalla, B. Camin, T. Buslaps, M. Di Michiel, H. Kaminski, A. Kottar, A. Pernack, W. Reimers, *Science* 308 (2005) 92–95.
- [24] A. Isaac, F. Sket, W. Reimers, B. Camin, G. Sauthoff, A.R. Pyzalla, *Mater. Sci. Eng. A* 478 (2007) 108–118.

- [25] K. Dzieciol, A. Isaac, F. Sket, A. Borbély, A.R. Pyzalla, Collected Proceedings TMS Conference, Characterization of Minerals, Metals and Materials, San Francisco, 15–19 February, 2009, p. 15.
- [26] A. Isaac, F. Sket, A. Borbély, G. Sauthoff, A.R. Pyzalla, *Pract. Metallography* 45 (2008) 242–245.
- [27] F. Sket, A. Isaac, K. Dzieciol, G. Sauthoff, A. Borbély, A.R. Pyzalla, *Scripta Mater.* 59 (2008) 558–561.
- [28] F. Garofalo, *Fundamentals of Creep and Creep-rupture in Metals*, Macmillan, New York, 1965, pp. 91–92 (Ref. [11]).